Rapid Beat Generation of Large-Scale Zonal Flows by Drift Waves: A Nonlinear Generic Paradigm

D. R. McCarthy,[1] C. N. Lashmore-Davies,[2] and A. Thyagaraja[2]
[1]*Southeastern Louisiana University, Hammond, Louisiana 70402, USA*
[2]*EURATOM/UKAEA Fusion Association, Culham Science Centre, Abingdon , OX14 3DB, United Kingdom*
(Received 9 June 2003; published 6 August 2004)

The generalized Charney-Hasegawa-Mima equation is unstable to a four wave modulational instability whereby a coherent, monochromatic drift wave can drive a band of modes and associated zonal flows unstable. Although initially the fastest growing modes dominate, a secondary nonlinear instability later drives the longest wavelength zonal flow and its associated sidebands at twice the growth rate of the fastest growing modulationally unstable modes. This results in a direct transfer from strongly unstable short wavelength modes to the weakly unstable long wavelength modes, which drains the short wavelength pump energy. A related but less efficient direct enstrophy cascade generates very short wavelength modes lying outside the band of modulationally unstable modes.

DOI: 10.1103/PhysRevLett.93.065004 PACS numbers: 52.35.Kt, 05.65.+b, 52.35.Mw

One of the most promising recent developments in magnetically confined fusion research has been the observation of transport barriers, in both the edge and the core plasmas. These barriers, which are characterized by highly sheared localized poloidal $\mathbf{E} \times \mathbf{B}$ flows, play a direct role in the suppression of turbulence by greatly inhibiting both particle and energy transport, thus leading to improved confinement. The causes of these "zonal flows" have been investigated by many authors.

One system that has been studied extensively with regard to the generation of zonal flows is the Charney-Hasegawa-Mima (CHM) equation, which was derived to describe low frequency electrostatic drift wave turbulence [1], as well as Rossby waves in atmospheric systems [2]. The CHM equation is appealing for the simple reason that it has successfully described a number of features of drift wave turbulence [3]. When the CHM equation is generalized to include a $k_y = 0$, zero frequency (in the linear approximation) component of the potential (i.e., the zonal flow), the system is unstable to a modulational instability that can generate zonal flows by means of a finite amplitude drift wave (generally known as the pump wave) interacting with other drift waves with shifted radial wave numbers (known as the sidebands) but the same *poloidal wave number*. The modulational instability has been studied by many authors [4–9], and appears to present a viable model for the generation of zonal flows, not just in plasmas, but also in geophysical systems where they were first noted [10].

Despite the simplicity of the two-dimensional generalized Charney-Hasegawa-Mima equation (GCHME), the mechanisms to be discussed are believed to be generic and relevant to more realistic systems. In particular, GCHME allows one to identify the means by which energy and enstrophy can be transferred directly in the early stages of the modulational instability to the slowly growing long and stable short wavelength fluctuations before the pump is depleted. This nonlinear equation for the electrostatic potential can be written as a pair of dimensionless, nonlinear coupled partial differential equations [Eqs. (63) and (64) in [8]], which read

$$\frac{\partial \bar{\phi}_{xx}}{\partial t} + \langle \hat{\Sigma}(x, y) \rangle_y = 0, \tag{1}$$

$$\frac{\partial \hat{f}}{\partial t} + \nabla \cdot (\mathbf{V}_0 \hat{f}) - \hat{\rho}^2 [\hat{\Sigma}(x, y) - \langle \hat{\Sigma}(x, y) \rangle_y] + \alpha \frac{\partial \tilde{\phi}}{\partial y} + \hat{\rho}^2 \frac{\partial \tilde{\phi}}{\partial y} \frac{\partial \overline{\phi}_{xx}}{\partial x} = 0, \tag{2}$$

where $\alpha = a/L_n$, a is the system size of the simulation, and L_n is the equilibrium gradient length scale. Furthermore, $c_s = (2T_e/m_i)^{1/2}$, $\Omega_i = eB/m_i c$, $\rho_s \equiv c_s/\Omega_i$, $\hat{\rho} = \rho_s/a$, $\hat{\Sigma}(x, y) = (\mathbf{z} \times \nabla \tilde{\phi}) \cdot \nabla \nabla_\perp^2 \tilde{\phi}$, $\hat{f} = (1 - \hat{\rho}^2 \nabla_\perp^2) \tilde{\phi}$, $\mathbf{V}_0 = (\rho_s c_s/a) \mathbf{z} \times \nabla \bar{\phi}$, the zonal flow. The y-averaged part of the normalized electrostatic potential is $\bar{\phi}$, while $\tilde{\phi}$ represents a drift wave fluctuation. All potentials are normalized to T_e/e. The space coordinates x, y are normalized to a and t to $a^2/(\rho_s c_s)$. Fully nonlinear fluid simulations are carried out by solving Eqs. (1) and (2) numerically [8].

We continue to concentrate on the simplest initial state consisting of a monochromatic pump wave, which we shall refer to as the drift wave pump with frequency ω_0 and wave number $\mathbf{k} = (k_x, k_y, 0) \equiv 2\pi(m_x, m_y, 0)$, where m_x, m_y are integers. The magnitude of the pump wave number is denoted by $k_0 = (k_x^2 + k_y^2)^{1/2}$. The modulational instability of such a pump wave has been described in detail in our earlier work [8]. As discussed therein, a zonal flow perturbation is treated as a zero frequency mode with wave number, $\mathbf{q} = (q, 0, 0) \equiv 2\pi(m_q, 0, 0)$, and m_q is an integer. Such a perturbation is generated by drift wave sidebands with wave numbers, $\mathbf{k}_\pm = (k_x \pm q, k_y, 0)$, beating with the pump wave. This produces a modulational instability with growing sideband and zonal flow perturbations draining energy from the pump wave. The growth rate of the modulational instability is given by

Eq. (49) in [8] and is illustrated in Fig. 6 of the same reference. For a given normalized pump wave amplitude A_0, there is a band of unstable zonal flow wave numbers q. It is clear that the wave number corresponding to maximum growth is $(q\rho_s)_{\max} = (c_s/V_d)|A_0|$, where we temporarily revert to dimensional units for clarity, using the definition of the diamagnetic drift velocity, $V_d = \alpha\rho_s c_s/a$. Initially, therefore, the wavelengths in the vicinity of $q_{\max}$ are expected to dominate, but the nature of the saturated nonlinear spectrum (the integral invariants found in [8] guarantee nonlinear saturation of the GCHME at long times) remains unclear. In the simulations described in our previous work [8], the nonlinearly saturated state contained many modes with many values of m_q, from the whole unstable band. For the case of $\alpha = 3$, although the longest wavelength zonal flow mode $m_q = 1$ was significant, the zonal flow was governed by the $m_q = 10$ mode (i.e., the mode with the maximum growth rate). The pronounced existence of the $m_q = 1$ mode (which is the weakest growing unstable mode in the system) presumably arose from the rather artificial (i.e., nongeneric) initial condition in which the *only* perturbations present were the upper and lower sidebands associated with the longest wavelength zonal flow mode. These sidebands were present initially at a level that was 1% of the pump amplitude corresponding to an amplitude level orders of magnitude above the thermal level and was more akin to a secondary pump. This raises the question as to whether these long wavelength modes are a characteristic of the true nonlinear state or are merely an artifact of our simplistic initial conditions. In order to study the evolution of the system under more physically realistic conditions, we consider an initial state in which all modes in the unstable band are present at a very low amplitude (10^{-6} of the pump amplitude). The dynamics of this initial state will be discussed numerically and analytically.

The results of a full numerical solution with the parameters $\alpha = 3$, $\hat{\rho} = 7.5 \times 10^{-3}$, $k_x = 2\pi m_x = k_y = 2\pi m_y = 2\pi \times 4$, and $A_0 = 0.01$ are shown in Figs. 1 and 2. Figure 1(a) shows surface plots of the Fourier amplitudes $\tilde{\phi}$ as functions of m_x (for $m_x \geq 0$) and time, while in Fig. 1(b) we plot the corresponding zonal flow amplitudes, $\bar{\phi}$. The pump wave corresponds to $m_x = 4$. The negative m_x values are not shown as the spectrum is symmetrical about $m_x = 4$. Figure 1(a) shows the modulationally unstable sidebands with the fastest growing modes clustered around $m_x = 13, 14$, the values corresponding to maximum growth (i.e., to $m_q = 9, 10$). Similarly, Fig. 1(b) shows the zonal flow modes dominated by maximum growth initially. However, an additional and unexpected feature shown clearly by both Figs. 1(a) and 1(b) is the appearance of a much faster growing, long wavelength perturbation (with $m_x = 5$; $m_q = 1$), which overtakes the short wavelength modes at a later stage of the simulation. The same behavior is also illustrated in Figs. 2(a) and 2(b). Figure 2(a) shows

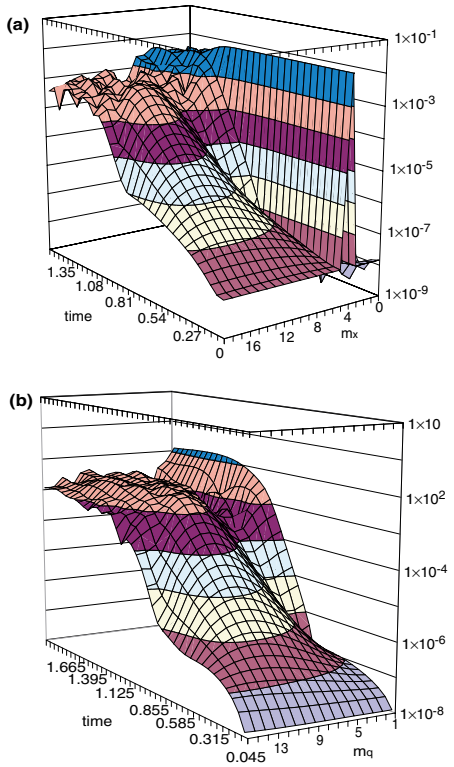

FIG. 1 (color online). Surface plots of the Fourier amplitudes (a) $\tilde{\phi}$ and (b) $\bar{\phi}$ as functions of time and m_x, m_q, respectively.

the rapid growth of the upper sideband amplitude associated with $m_q = 10$ and the slow initial growth of the upper sideband amplitude associated with $m_q = 1$. The latter exhibits an abrupt transition to a fast growing mode at approximately $t = 0.5$ and eventually overtakes the short wavelength mode at $t = 0.9$. Note that this happens before pump depletion begins, at around $t = 1$. The curve labeled "ratio" will be discussed later. In Fig. 2(b) we plot the zonal flow amplitudes of the $m_q = 10$ and $m_q = 1$ modes. It is clear that it too shows the same behavior as the sidebands described in Fig. 2(a).

Let us now reconsider the analysis leading to the modulational instability, but with an additional feature suggested by the results from the numerical simulation. The pump wave is again assumed to have the form given by Eq. (26) in [8] with $\omega_0 = \alpha k_y/(1 + \hat{\rho}^2 k_0^2)$ normalized to $c_s\rho_s/a^2$. Instead of considering a representative zonal flow wave number, we introduce two zonal flow wave numbers, q and p, where we assume, without loss of generality, $q > p > 0$. In the numerical simulations, $q = 2\pi m_q$, $p = 2\pi m_p$, and $m_q > m_p > 0$. Both q and p are assumed to be in the band of modulationally unstable wave numbers, and we shall concentrate on the case where both are initially in the vicinity of the fastest growing mode. Clearly the zonal flow with mode number q is associated with unstable sidebands, $(k_x \pm q, k_y, 0)$, which grow at the rate γ_q given by Eq. (47) in [8]. We denote this zonal flow and sidebands by B_q and $a_{k_x \pm q, k_y} \equiv a_{\pm q}$. Similarly, the zonal flow with wave number p (and its

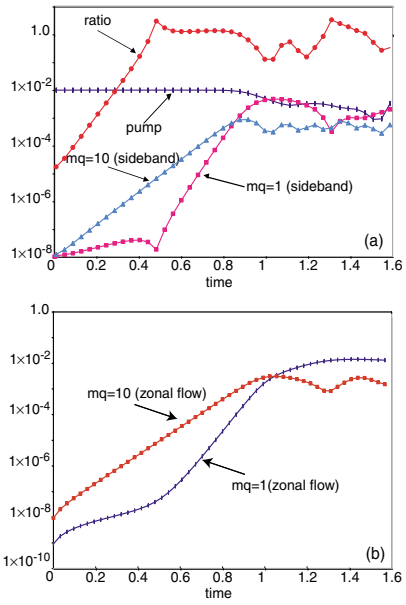

FIG. 2 (color online). Time development of (a) the pump amplitude, upper sidebands with $m_q = 1, 10$, and ratio of amplitudes; (b) zonal flow amplitudes for $m_q = 1, 10$.

sidebands) grows at γ_p given by the same dispersion equation. This zonal flow and its sidebands are denoted by B_p and $a_{\pm p}$. The fastest growing, modulationally unstable modes at first dominate the evolution of the system. However, the longest wavelength, $m_q = 1$, zonal flow mode that is driven initially by $A_0^* a_1$ and $A_0 a_{-1}^*$ is also driven by the beating of the fastest growing modes through the terms $a_q a_p^*$ and $a_{-q}^* a_{-p}$ to produce the difference wave number, $q - p$. Both the driving terms grow at the sum of the growth rates, $\gamma_q + \gamma_p$. Similar arguments apply to the sidebands $a_{\pm 1}$. The long wavelength sidebands are initially driven by $A_0 B_{\pm 1}$, where $B_{-1} = B_1^*$, but they are also driven by the zonal flows $B_{q,p}$ and the sidebands $a_{\pm q}$ and $a_{\pm p}$. Although the pump wave is initially much larger than all other modes, the nonlinear driving terms such as $a_q a_p^*$ can become more important than those involving the pump because a_1 is so slowly growing and a_q and a_p grow relatively much more rapidly. This qualitative discussion is now translated into appropriate differential equations for the amplitudes involved in this secondary nonlinear interaction. To facilitate the analysis we introduce the difference and sum wave numbers, $\tau = q - p$, $\sigma = q + p$, and the associated "triads," $(B_\tau, a_\tau, a_{-\tau})$, $(B_\sigma, a_\sigma, a_{-\sigma})$. The modified equations follow from Eqs. (1) and (2) in a manner similar to Eqs. (38)–(40) in [8]. Thus we have, collecting the homogeneous terms on the left and the "driving"terms dependent on the q, p triads on the right, the following evolution equations for the long wavelength triad, $(B_\tau, a_\tau, a_{-\tau})$:

$$\frac{dB_\tau}{dt} - \tau k_y \frac{(k_\tau^2 - k_0^2)}{\tau^2} a_\tau A_0^* + \tau k_y \frac{(k_{-\tau}^2 - k_0^2)}{\tau^2} a_{-\tau}^* A_0 = F_\tau^B, \tag{3}$$

where $F_\tau^B = \tau k_y \frac{(k_q^2 - k_p^2)}{\tau^2} a_q a_p^* + \tau k_y \frac{(k_{-p}^2 - k_{-q}^2)}{\tau^2} a_{-p} a_{-q}^*$.

$$\frac{da_\tau}{dt} + i\delta_\tau a_\tau - \tau k_y \frac{[1 + (k_0^2 - \tau^2)\hat{\rho}^2]}{[1 + k_\tau^2 \hat{\rho}^2]} A_0 B_\tau = F_\tau^+, \tag{4}$$

where $F_\tau^+ = q k_y \frac{[1+(k_{-p}^2 - q^2)\hat{\rho}^2]}{[1+k_\tau^2\hat{\rho}^2]} a_{-p} B_q - p k_y \frac{[1+(k_q^2 - p^2)\hat{\rho}^2]}{[1+k_\tau^2\hat{\rho}^2]} \times a_q B_{-p}$.

$$\frac{da_{-\tau}}{dt} + i\delta_{-\tau} a_{-\tau} + \tau k_y \frac{[1 + (k_0^2 - \tau^2)\hat{\rho}^2]}{[1 + k_{-\tau}^2 \hat{\rho}^2]} A_0 B_{-\tau} = F_\tau^-, \tag{5}$$

where $F_\tau^- = p k_y \frac{[1+(k_{-q}^2 - p^2)\hat{\rho}^2]}{[1+k_{-\tau}^2\hat{\rho}^2]} a_{-q} B_p - q k_y \frac{[1+(k_p^2 - q^2)\hat{\rho}^2]}{[1+k_{-\tau}^2\hat{\rho}^2]} \times a_p B_{-q}$.

Note that $\delta_{\pm\tau} \equiv \omega_{\pm\tau} - \omega_0$, $\omega_{\pm\tau} = \alpha k_y/(1 + k_{\pm\tau}^2 \hat{\rho}^2)$, $k_{\pm\tau}^2 = (k_x \pm \tau)^2 + k_y^2$. Similarly, $k_{\pm q}^2 = (k_x \pm q)^2 + k_y^2$, $k_{\pm p}^2 = (k_x \pm p)^2 + k_y^2$. It should be apparent that Eq. (5) follows from Eq. (4) by merely changing $q \to -q$, $p \to -p$, $\tau \to -\tau$. Note that $B_{-q} = B_q^*$. It follows that the homogeneous part of the above equations is identical with Eqs. (38)–(40) in [8]. The complementary solution to Eqs. (3)–(5) gives the slow growing, modulationally unstable solution. An approximate solution of the modified equations can be obtained by treating the additional coupling terms as inhomogeneous forcing effects. This is justified because the p, q triads grow at a much faster rate, in the initial modulational instability, as compared with the $\tau = q - p$ triad. Making use of the modulational instability solutions for the driving triads, (B_q, a_q, a_{-q}), (B_p, a_p, a_{-p}), it is clear that all the inhomogeneous terms have the same time dependence given by $\exp[i(\Omega_q - \Omega_p)t + (\gamma_q + \gamma_p)t]$, where Ω_q and Ω_p are the real parts of the solution of the modulational instability dispersion relation [ie., Eq. (47) in [8]]. Hence the particular integral will be proportional to $\exp(\gamma_q + \gamma_p)t$, growing at close to twice the *maximum* growth rate for the original modulational instability. The particular integral will therefore dominate once the q, p triads have grown sufficiently such that products like $a_q a_p^*$ become larger than, say, $a_\tau A_0^*$. Thus, although the pump amplitude is *initially* much larger than all other amplitudes, the numerical solutions show that this condition of secondary dominance is satisfied, well before the pump depletes. Hence the long wavelength triad, $(B_\tau, a_\tau, a_{-\tau})$, grows at the above greatly enhanced rate (relative to its initial modulational instability growth rate, γ_τ). It is also clear that the most strongly driven mode is the longest wavelength one, corresponding to $m_q - m_p = 1$. This is because the beating modes are closer together in wave number space and can therefore both be very close to maximum growth. Furthermore, it is evident that other neighboring modes in the vicinity of the maximum growth contribute additively to the longest wavelength mode. Hence, the energy from the pump cascades through the beating of the fastest growing modes to the (initially) slowest growing mode.

There is, in addition, a further possibility. The fast growing modes that beat together to drive up the longest wavelength modes also drive a *short* wavelength triad

$(B_\sigma, a_\sigma, a_{-\sigma})$, where $\sigma = q + p$. These short wavelength modes lie in the stable region of wave number space for the modulational instability. The above mechanism drives them at the rate $\gamma_q + \gamma_p$, although the driving term oscillates at the higher frequency $\Omega_q + \Omega_p$. Such strongly unstable modes were observed in the simulations, with identical growth rates to the corresponding long wavelength triads.

The system of equations, Eqs. (3)–(5), is able to account for the most striking features of the simulations shown in Figs. 1 and 2. A linear fit of the data gives the growth rates of the three fastest waves as $\gamma_9 = 13.36$, $\gamma_{10} = 13.58$, and $\gamma_{11} = 13.41$, while the nonlinear growth rate of the $m_q = 1$ sideband is $\gamma_1 = 26.63$, thus verifying that the nonlinear growth rate of this mode is the sum of the two fastest growing modes. The condition for the abrupt change in the growth of the slowest growing modes can be obtained from Eq. (3). This occurs when the ratio $(k_q^2 - k_p^2)a_q a_p^*/(k_\tau^2 - k_0^2)a_\tau A_0^* > 1$ [cf. Fig. 2(a)]. This ratio is plotted in Fig. 2(a) as a function of time. Figures 2(a) and 2(b) clearly show the pronounced transition from the slowly growing modulationally unstable regime to the very fast nonlinear growth regime. This happens just after this condition is met for both the $m_q = 1$ zonal flow and its associated upper sideband. We note that once the ratio reaches unity it hovers around this value. This is evidently because the two terms in the ratio then grow at the same rate due to the enhancement of the growth of the long wavelength modes to $2\gamma_{\max}$. It can be seen from Fig. 2(b) that in the saturated state the $m_q = 1$ zonal flow potential is much larger than the $m_q = 10$ potential. The zonal flow is proportional to dB_q/dx, however, and detailed study shows that the fine structure of the flow is influenced by the shortwave modes (e.g., $m_q = 10$) while the longest wavelength $m_q = 1$ mode has a significant effect on the net asymmetry between the positive and the negative flows.

Reference [3] used a sequence of three-wave interactions derived from the Charney-Hasegawa-Mima equation to give a heuristic description of the generation of a zonal flow relevant to transport reduction in magnetized plasmas and atmospheric systems. The present work utilizes the GCHME and, through the more general (and robust) modulational instability, gives a detailed and quantitative account of how a dramatically enhanced growth of the long wavelength zonal flow results from a finite amplitude monochromatic drift wave. The key new ingredient, observed first by means of an exact numerical simulation of the GCHME, is a secondary instability that arises from the modulationally most unstable modes and causes a direct transfer of the pump energy through these fastest growing modes to the longest wavelengths. This produces an abrupt change in the evolution of the longest wavelength mode from a weakly growing mode to one growing at $2\gamma_{\max}$, where $\gamma_{\max}$ is the maximum growth rate of the initial modulational instability. A similar mechanism leads to the growth, also at $2\gamma_{\max}$, of short wavelength modes that are initially stable. Note that other long wavelength modes (e.g., $m_q \geq 2$) are also driven by the beat mechanism at slightly later times at somewhat lower rates. Clearly any higher order interactions between unstable modes can play a role only when the product of two unstable amplitudes exceeds the product of the pump amplitude and the unstable mode. Although these can have fast growth, our simulations show that before pump depletion these modes are not significant. The beat mechanism is clearly important for the evolution to a saturated turbulent state and to the production of the spectrum of fluctuations. It is also clear that the mechanism is generic and qualitatively explains phenomena in more realistic systems (e.g., zonal flow and dynamo effects studied in [11]). The GCHME is possibly the simplest nonlinear system that exhibits the phenomenon of rapid zonal flow generation or inverse spectral cascading by beating modulationally unstable short wavelength drift waves. Although conservative, and therefore the saturation mechanisms operative at high wave numbers are likely to be different in GCHME from more realistic driven-dissipative systems, its dynamical and spectral behavior at long wavelengths are remarkably similar to those found in more elaborate two-fluid models [11]. The ultimate saturated spectrum in the GCHME is controlled by its integral invariants [8], and its characterization is beyond the scope of this work.

This work was supported by the U.S. Department of Energy Grant No. DE-FG02-96ER-54370, the Louisiana Educational Quality Support Fund, Southeastern Louisiana University, EURATOM, and the EPSRC (U.K.).

[1] A. Hasegawa and K. Mima, Phys. Fluids **21**, 87 (1978).
[2] J. C. Charney, J. Atmos. Sci. **28**, 1087 (1971).
[3] A. Hasegawa, C. G. McClennan, and Y. Kodama, Phys. Fluids **22**, 2122 (1979).
[4] A. I. Smolyakov, P. H. Diamond, and V. I. Shevchenko, Phys. Plasmas **7**, 1349 (2000).
[5] L. Chen, Z. Lin, and R. White, Phys. Plasmas **7**, 3129 (2000).
[6] P. N. Guzdar, R. N. Kleva, and L. Chen, Phys. Plasmas **8**, 459 (2001).
[7] G. Manfredi, C. M. Roach, and R. O. Dendy, Plasma Phys. Controlled Fusion **43**, 825 (2001).
[8] C. N. Lashmore-Davies, D. R. McCarthy, and A. Thyagaraja, Phys. Plasmas **8**, 5121 (2001).
[9] J. Li and Y. Kishimoto, Phys. Plasmas **9**, 1241 (2002).
[10] G. P. Williams, J. Atmos. Sci. **35**, 1399 (1978).
[11] M. R. de Baar, A. Thyagaraja, P. J. Knight, G. M. D. Hogeweij, and N. J. Lopes Cardozo, J. Plasma Fusion Res. **5**, 318 (2002).